Infrared Spectroscopy of Multiply Charged Metal Ions: Methanol-Solvated Divalent Manganese 18-Crown-6 Ether Systems

Jason D. Rodriguez and James M. Lisy*

Department of Chemistry, University of Illinois at Urbana−Champaign, Urbana, Illinois 61801

Received: March 17, 2009; Revised Manuscript Received: April 24, 2009

We have developed an electrosonic spray ionization source to successfully generate divalent Mn^{2+}(18-crown-6)$(CH_3OH)_{1-3}$ complexes in the gas phase. These complexes have been investigated using infrared predissociation spectroscopy in both the CH and OH stretching regions and with density functional theory calculations. To resolve complications from overlapping bands in the CH stretching region due to CH_3OH and 18-crown-6 CH stretching modes along with strongly perturbed OH stretching modes, we have used $\mathbf{d_1}$ and $\mathbf{d_4}$ methanol substitution. For $n = 1$, the $Mn^{2+}\cdots$18-crown-6 geometry is highly distorted from its gas-phase neutral configuration in order to maximize favorable electrostatic interactions between the 18-crown-6 macrocyclic oxygens and Mn^{2+}. For $n = 2$ and 3, $CH_3OH\cdots CH_3OH$ and $CH_3OH\cdots$18-crown-6 interactions compete with the $Mn^{2+}\cdots$18-crown-6 interaction, as evidenced by intense hydrogen-bonded OH stretching modes shifted over 500 cm^{-1} to lower frequency.

Introduction

Chemical phenomena such as dissociative charge transfer[1] have made the generation of gas-phase multivalent solvated metal ions challenging. While great advances have been made in the production and subsequent spectroscopic investigation of multiply charged species[2,3] only a few vibrational/infrared spectroscopic studies have been reported.[4−9] Two successful methods for generation have been the "pick up" technique[10] and electrospray ionization (ESI).[11] The latter method, first used by Kebarle to conduct mass spectrometric studies on divalent alkaline earth metal ions,[12] has often been a more attractive option due to its "soft" nature and ease of use. We have developed a modified electrosonic spray ionization[13] (ESSI) source to generate methanol-solvated Mn^{2+} complexes with 18-crown-6 ether (18c6). Crown ethers, an important class of molecules, have been shown to selectively bind to alkali metal ions in solution.[14] This selectivity has been theorized to be due to a strong correlation between the size of the metal ion and the crown ether cavity.[15] However the selectivity trends observed in the condensed phase do not transfer to the gas phase. This suggests that condensed phase binding affinities of metal ion−crown ether complexes may not be due to simple host−guest best-fit matching but rather to a balance of all noncovalent interactions.[16] Insight into these interactions may lead to the design and development of new, highly selective crown ethers that can be used in such applications as drug delivery[17] and nuclear waste management.[18] We report our effort to broaden the study of solvated metal ion−crown ether systems to multivalent transition metal ions, with their rich and often unique chemistry. Complexation with 18c6 preserves the charge[19] of Mn^{2+}. Unlike other systems where charge reduction/transfer has restricted experiments to a minimum cluster size,[20] the stabilization by 18c6 allows us to start from the monosolvated cluster. We have characterized the infrared predissociation (IRPD) spectra of Mn^{2+}(18c6)$(CH_3OH)_n$, $n = 1-3$, in both the CH and OH stretching regions.

* Corresponding author information: tel, (217) 333-2898; fax, (217) 244-3186; e-mail, j-lisy@uiuc.edu.

Experimental and Computational Methods

Experimental Methods. A custom-built ESSI source, shown in Figure 1, was used to transfer Mn^{2+}(18c6)$(CH_3OH)_n$ complexes in the gas phase. Our ESSI is similar to a source reported by Cooks and co-workers[13] with a few key differences. First, our ESSI source is more consistent with a traditional electrospray source[11] inasmuch as it uses an electrospray needle biased at high voltage (+4−5 kV) to achieve charge separation and produce the fine spray of ions at the tip of an electrospray needle. The source reported by Cooks[13] biases the *syringe* needle to achieve charge separation and relies on fused silica capillary tubing to deliver the spray to atmospheric conditions. Second, the pressure of the sheath gas used in our source (50−120 psi) is lower than the pressures (116−362 psi) reported by Cooks.[13] High sheath gas flow rates are commonly used in sonic spray ionization[21] but not in traditional electrospray. In our ESSI source, this high-pressure sheath gas has provided a 5-fold improvement in our ion beam intensity over a traditional electrospray source, which was also tested.

A syringe pump (Harvard Apparatus model 22) is used to pass solutions (0.1−1 mM) to our ESSI source. Solutions of $MnCl_2\cdot 4H_2O$ and 18-crown-6 (Aldrich) are prepared in spectroscopic grade methanol. The ions produced by the ESSI source enter our source chamber via a 0.030 in. i.d. heated capillary (80−120 °C). Upon exiting the capillary the ions are sampled by a 0.50 mm diameter skimmer and are guided by a 25 cm octapole ion guide (OPIG) (peak-to-peak voltage, 200−700 V; rf frequency, 1.2 MHz) through the length of our source chamber. Cluster ions enter an ion guiding chamber via a 2.0 mm diameter skimmer and are guided to the detector chamber by a second OPIG (peak-to-peak voltage, 200−700 V; rf frequency, 1.2 MHz) and a stack of electrostatic lenses. In the detector chamber, the parent cluster ions of interest are mass selected by the first quadrupole. These mass-selected clusters then enter the second quadrupole (rf-only), which serves as an ion guiding quadrupole. While in the second quadrupole, the cluster ions interact with the output of a tunable infrared laser (Laser Vision OPO/A) pumped by a 10 Hz Nd:YAG laser.

10.1021/jp902381y CCC: $40.75
Published on Web 05/19/2009

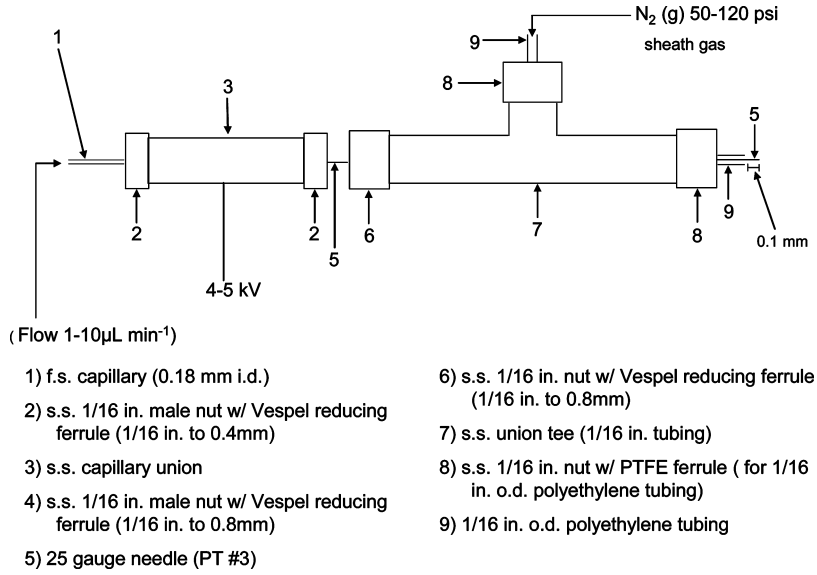

Figure 1. Custom electrosonic spray ionization (ESSI) source. The source uses a needle (5) biased at high voltage to achieve charge separation. The resulting spray is stabilized with the use of a nitrogen sheath gas.

Fragment ions resulting from single-photon photodissociation are mass analyzed by the third quadrupole, and the action spectrum is recorded as a function of laser frequency. Since the binding energy of 18c6 in these systems is predicted to be ~1200 kJ/mol at the B3LYP/6-31+G* level of theory (vide infra), all of the spectra were acquired monitoring the loss of CH_3OH. The binding energy of CH_3OH in these systems is estimated to be ~60−90 kJ/mol at the same level of theory. Although this exceeds the available photon energy (~31−45 kJ/mol) in the region studied, ESSI-generated complexes have sufficient internal energy[22] to facilitate the loss of CH_3OH following the absorption of a photon. A three-point averaging procedure was applied to smooth the experimental spectra. Further details of our apparatus and experimental methods have been described elsewhere.[23]

Computational Methods. To assist in the interpretation of our experimental results, we performed quantum chemical calculations on the $Mn^{2+}(18c6)(CH_3OH)_n$ complexes. We generated starting geometries of candidate structures using the Spartan 02[24] software package. Geometry optimizations and harmonic vibrational frequency calculations were then carried out using density functional theory (DFT) at the B3LYP/6-31+G* level using Gaussian 03.[25] The fully optimized structures of the $Mn^{2+}(18c6)(CH_3OH)_n$ candidate conformers are shown in Figure 2. The graphical representation of these structures were generated using Molden[26] and are based on the geometry optimizations. Simulated IR spectra were generated using SWizard.[27] Gaussian line shapes (fwhm; free OH stretches, 15 cm^{-1}; hydrogen-bonded OH stretches, 120 cm^{-1}; CH stretches, 20 cm^{-1}) were used to model the experimental features in the simulated spectra. Calculated frequencies were scaled to facilitate comparison with experiments. Frequencies in the CH stretching region were scaled by 0.953, while two scaling factors were used in the OH stretching region, 0.971 for free OH stretches and 0.962 for hydrogen-bonded OH stretches. Free energies were calculated using the THERMO.PL[28] script using the output of the vibrational frequency calculations.

Results and Discussion

The IRPD spectra for $Mn^{2+}(18c6)(CH_3OH)_{1-3}$ in the 2600−3700 cm^{-1} region are shown in Figure 3. There is an obvious difference between the $n = 1$ and $n = 2$, 3 spectra. The intense broad bands in the 2700−3300 cm^{-1} region exhibited by $Mn^{2+}(18c6)(CH_3OH)_{2,3}$ are due to methanol hydrogen-bonded OH bands (vide infra). We will now consider the experimental spectrum for each cluster with simulated spectra derived from DFT calculated harmonic frequencies.

The spectrum of $Mn^{2+}(18c6)(CH_3OH)_1$ has two sets of features in regions nominally associated with the CH and OH stretching regions. It is shown in Figure 4 along with the

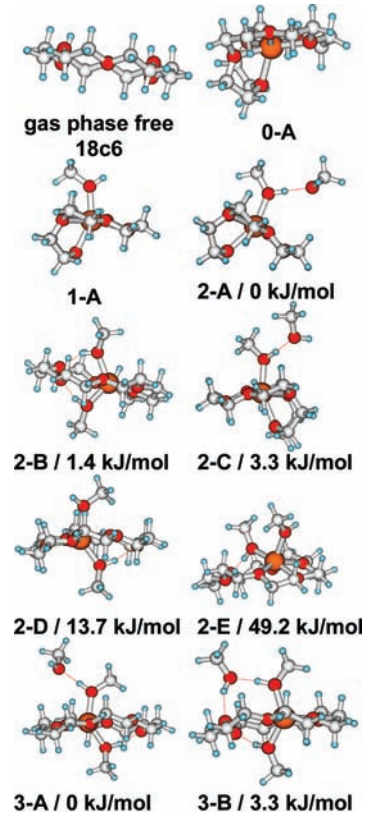

Figure 2. Fully optimized geometries of candidate $Mn^{2+}(18c6)(CH_3OH)_n$ conformers at the B3LYP/6-31+G* level of theory. Structures corresponding to neutral 18c6 and the bare $Mn^{2+}(18c6)$ are also given for reference. The relative Gibbs free energies ($\Delta G°$) are also given at 298 K.

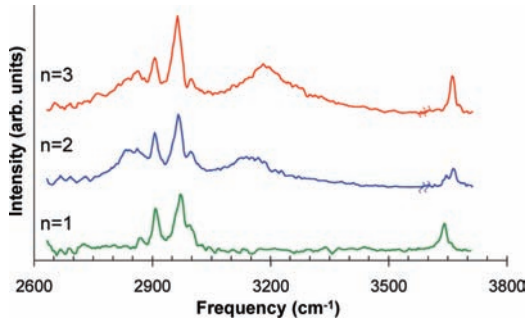

Figure 3. Experimental IRPD spectral summary of $Mn^{2+}(18c6)-(CH_3OH)_n$ complexes. The experimental spectra for $n = 2$ and 3 in the free OH region, 3600−3700 cm^{-1}, are enhanced by a factor (×3) to emphasize the interesting singlet−doublet−singlet progression.

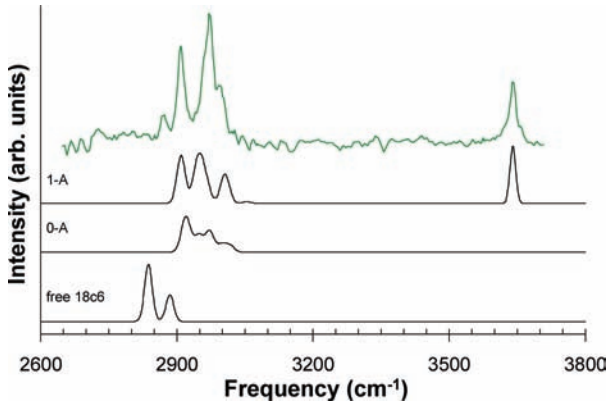

Figure 4. IRPD spectrum of $Mn^{2+}(18c6)(CH_3OH)_1$ in the 2600−3800 cm^{-1} region. The simulated spectra for the $Mn^{2+}(18c6)(CH_3OH)_1$ complex (**1-A**), the unsolvated $Mn^{2+}(18c6)$ complex (**0-A**), and gas phase free 18c6 complex based on the B3LYP/6-31+G* harmonic frequency calculations are also shown.

calculated spectrum based on conformer **1-A** in Figure 2. In the OH stretching region, there is a single sharp peak at 3643 cm^{-1} in the experimental spectrum from an OH group that is not involved in a hydrogen bond. This "free" OH stretch is shifted to lower frequency by about 40 cm^{-1} compared to gas-phase neutral methanol.[29] The absence of any intense broad features in the hydrogen bonding region, below 3600 cm^{-1}, indicates there is no interaction between the methanol and the 18c6 ether via the OH group. For $n = 1$, there are two prominent noncovalent interactions; the $Mn^{2+}\cdots$18c6 interaction that is apparent from structure **1-A**, where the 18c6 is distorted to wrap around the dication, and the $Mn^{2+}\cdots CH_3OH$ interaction via the oxygen on the methanol. The $Mn^{2+}\cdots$18c6 interaction seems to be the more dominant interaction since it significantly distorts the structure of 18c6 from its neutral gas phase geometry (shown in Figure 2).

To gauge the effect of Mn^{2+} on the vibrational modes of 18c6, we scanned the CH stretching region from 2600 to 3000 cm^{-1}. The simulated IR spectra for the unsolvated $Mn^{2+}(18c6)$ complex (**0-A**) and neutral gas phase free 18c6 (structures shown in Figure 2) are also shown in Figure 4. The series of simulated spectra clearly show that the 18c6 vibrations are perturbed significantly when the macrocycle binds Mn^{2+}. However, only slight differences in the CH stretching region are observed when going from the unsolvated species (**0-A**) to the complex containing one CH_3OH (**1-A**). Since both 18c6 and methanol have CH stretches, deuterated studies using both CD_3OD (**d_4**) and CH_3OD (**d_1**) methanol were performed to eliminate the ambiguity in the CH stretching region and are shown in Figure 5. Both sets of spectra in Figure 5 have three prominent features

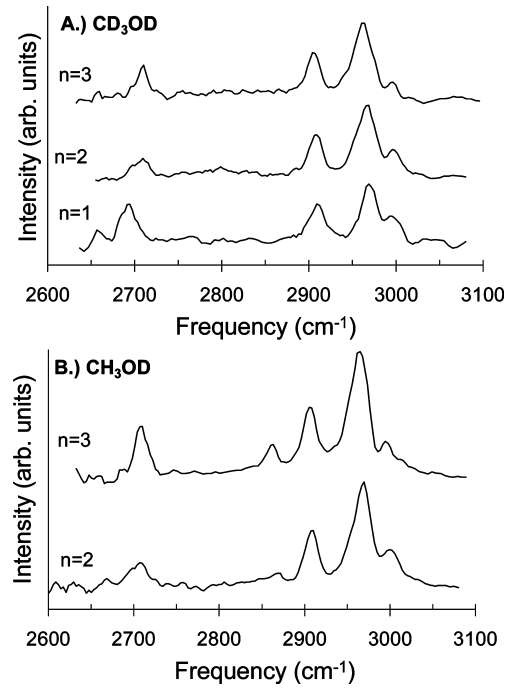

Figure 5. IRPD spectra of $Mn^{2+}(18c6)(methanol)_n$ in the 2600−3100 cm^{-1} region. Panel A shows the spectra for CD_3OD (**d_4**) substituted methanol and panel B shows the spectra for CH_3OD (**d_1**) substituted methanol. The peak at ∼2865 cm^{-1} is likely due to a methanol CH stretch.

located at 2908, 2970, and 2996 cm^{-1}. Since only 18c6 has CH modes in the methanol-d_4 spectra, these transitions are due to 18c6 CH stretch vibrations. On the basis of the DFT calculations we can make general assignments of the features at 2909 and 2970 cm^{-1} to the symmetric and asymmetric stretches, respectively, of the 18c6 methylene groups. These modes are shifted to higher frequency by about 40 and 50 cm^{-1}, respectively, compared to uncomplexed neutral 18c6.[30] The feature at 2996 cm^{-1} will be discussed later. All the spectra for both CD_3OD and CH_3OD also have a feature at ∼2690 cm^{-1} which is the free OD stretch. This vibration is shifted ∼30 cm^{-1} to lower frequency from the gas-phase neutral value of 2720 cm^{-1} for the **d_1** species and 2725 cm^{-1} for the **d_4** species.[31]

The CH_3OD spectra, shown in panel B, have an additional feature at ∼2865 cm^{-1}, which is not present in the CD_3OD spectra. This transition must be due to a methanol CH stretch and, based on its frequency, is likely due to the ν_3 mode[29] (CH_3 symmetric stretch). The other CH stretching modes of methanol overlap 18c6 methylene vibrations and cannot be resolved or identified. The deuterium studies confirm that the peaks at 2908 and 2970 cm^{-1} in the $Mn^{2+}(18c6)(CH_3OH)_1$ system (shown in Figure 4) are due to the symmetric and asymmetric methylene stretches, respectively, of 18c6. The additional feature in $Mn^{2+}(18c6)(CH_3OH)_1$ at 2870 cm^{-1} can be assigned to the ν_3 vibration of methanol.

The IRPD spectrum for $Mn^{2+}(18c6)(CH_3OH)_2$ along with simulated spectra obtained from the DFT harmonic vibrational frequencies are shown in Figure 6. The IRPD spectrum for $n = 2$ is markedly different from $n = 1$, with two broad peaks centered at 2840 and 3150 cm^{-1}. The intensity and breadth of these peaks are consistent with those expected for hydrogen-bonded OH stretches. The feature at 3150 cm^{-1} occurs in a region where a strong hydrogen-bonded OH stretch may be expected, but the 2840 cm^{-1} feature overlaps the CH stretching region. However since both series of deuterated spectra in Figure

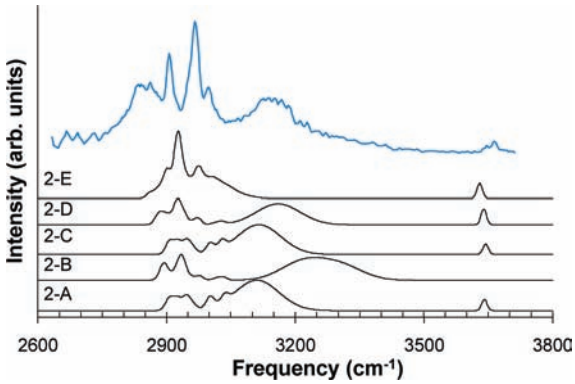

Figure 6. IRPD spectrum of $Mn^{2+}(18c6)(CH_3OH)_2$ in the 2600−3700 cm^{-1} region. The calculated spectra based on the harmonic vibrational frequencies of five possible conformers (B3LYP/6-31+G*) are shown. None of the calculated spectra are able to model the lower frequency region of the experimental spectrum.

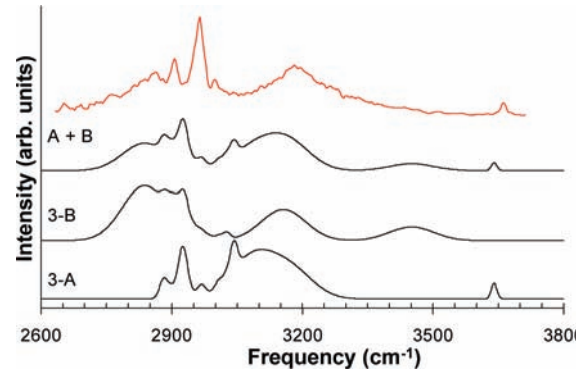

Figure 7. IRPD spectrum of $Mn^{2+}(18c6)(CH_3OH)_3$ in the 2600−3700 cm^{-1} region. The calculated spectra based on the harmonic vibrational frequencies of structures **3-A** and **3-B** (B3LYP/6-31+G*) are shown. The A + B total spectrum shows that the calculations agree well with the experiment.

5 lack the 2840 cm^{-1} feature, we conclude that both broad features present in $n = 2$ are due to OH transitions.

Unlike $n = 1$ where only one stable conformer was found, five stable conformers were identified for $n = 2$ and are also shown in Figure 2 along with their relative free energies. The three lowest energy conformers are **2-A**, **2-B**, and **2-C**, which all lie within 3.3 kJ mol^{-1} of each other. Conformers **2-A** and **2-C** are nearly identical, except for a slight difference in the orientation of the methanols. These two conformers seem to continue the trends observed in **1-A**, where 18c6 is highly distorted due to the $Mn^{2+}\cdots$18c6 interaction. In conformer **2-B** the $Mn^{2+}\cdots$18c6 interaction appears to be somewhat weakened by the direct interaction of the Mn^{2+} with the methanols in a sandwich-type orientation above and below the 18c6 plane. This opening of the 18c6 ring allows for the onset of $CH_3OH\cdots$18c6 interactions with the formation of both top and bottom hydrogen bonds that allow the ring to assume a more open configuration. The other two conformers, **2-D** and **2-E** are higher in relative energy by 13.7 and 49.2 kJ mol^{-1}, respectively. Conformer **2-D** is similar to **2-B** except the top methanol orientation is rotated so that a $CH_3OH\cdots$18c6 hydrogen bond is not possible.

On the basis of the simulated spectra and the relative energy ordering, the three lowest energy conformers are likely present in our experiment. In the experimental spectrum for $n = 2$, in addition to the hydrogen-bonded feature at 3150 cm^{-1}, there appears to be an area of weaker intensity present in the 3200−3400 cm^{-1} region. The 3150 cm^{-1} feature likely arises from conformers **2-A** and **2-C** and is due to the strong $CH_3OH\cdots CH_3OH$ hydrogen bond present in both conformers. The area of weaker hydrogen-bonded intensity is due mostly to population of conformer **2-B** in the experiment as its simulated spectrum readily reproduces the 3200−3400 cm^{-1} region in the experiment. Conformer **2-D**, despite its higher relative energy, is a bit harder to assign since it has does not contain a unique spectral feature and contains hydrogen-bonded features that have intermediate spectral properties between **2-B** and **2-C**. Conformer **2-E** is 49.2 kJ mol^{-1} higher in relative energy, making its existence in our experiment unlikely. The likely existence of the three lowest energy conformers in our experiment gives us insight into nature of the $Mn^{2+}\cdots$18c6, $CH_3OH\cdots CH_3OH$, and $CH_3OH\cdots$18c6 interactions and their interdependence on one another. The $CH_3OH\cdots CH_3OH$ interaction is present only when the $Mn^{2+}\cdots$18c6 interaction dominates. This is apparent in conformers **2-A** and **2-C** where the 18c6 ring is wrapped around Mn^{2+}. The second-shell methanol simply has no other binding sites available and binds to the first-shell methanol. Only when the $Mn^{2+}\cdots$18c6 interaction is weakened and the 18c6 ring becomes less distorted does the $CH_3OH\cdots$18c6 interaction manifest itself.

In the CH stretching region the features attributed to the symmetric and asymmetric stretches of 18c6 are nearly unchanged from $n = 1$(see Figure 3). However, none of the conformers discussed thus far are able to satisfactorily replicate the broad feature, at 2840 cm^{-1}, which must be due to the OH group, based on the $\mathbf{d_4}$ and $\mathbf{d_1}$ spectra in Figure 5. One possible explanation for this is that the broad feature is due to anharmonic coupling between the hydrogen-bonded OH stretch and OH in-plane bend overtone ($2\nu_6$), which would not show up in harmonic vibrational frequency calculations. Previous work done by Johnson and co-workers on $X^-(H_2O)_1$ complexes indicates that OH bend overtones may "borrow" intensity via a Fermi resonance from the hydrogen-bonded OH transition.[32] The calculated in-plane bend (ν_6) is present between 1340 and 1476 cm^{-1} for all methanols in $n = 2$ conformers. This would put $2\nu_6$ in the ∼2680−2942 cm^{-1} region. The 2840 cm^{-1} broad feature present in the experiment would fall within this region. The splitting between $2\nu_6$ and the position of the calculated hydrogen bond frequencies is less than 200 cm^{-1} for **2-A** and **2-C**, indicating that for these conformers coupling between the hydrogen-bonded OH transition and the $2\nu_6$ mode of the methanol OH vibration is possible and may manifest itself as the broad feature at 2840 cm^{-1}.

The free OH region is also intriguing in that for $n = 2$, there are two distinct free OH features, shown in Figure 3. The lower frequency peak is located at 3645 cm^{-1}, similar to $n = 1$, and the higher frequency peak is located just above 3660 cm^{-1}. The origin of this doublet is additional evidence of multiple conformers present in the experiment. One possible explanation for the doublet is that the higher frequency peak is due to a second-shell methanol that is further away from the ion while the lower frequency peak is due to a first-shell methanol closer to the ion. On the basis of this reasoning, conformers **2-A** and **2-C**, which both contain second-shell methanols with a free OH group, give rise to the higher-frequency free OH feature observed experimentally, while conformer **2-D**, with a first-shell methanol, could be responsible for the lower-frequency free OH feature.

The IRPD spectrum for $Mn^{2+}(18c6)(CH_3OH)_3$ along with simulated spectra obtained from the DFT harmonic vibrational frequencies is shown in Figure 7. The general trends observed in $n = 2$ are replicated for $n = 3$. Again, there are two broad features that dominate the spectrum at 2865 and 3185 cm^{-1}.

These are slightly shifted to higher frequency compared to $n = 2$. The two stable conformers found, **3-A** and **3-B**, lie within 3.3 kJ mol^{-1} of each other, making both conformers likely contributors to the experimental spectrum. The total calculated spectrum and the IRPD spectrum are in strong agreement, replicating even the broad feature at 2865 cm^{-1}. This feature arises from the $CH_3OH\cdots CH_3OH$ hydrogen bond in **3-B**. In light of this result, a similar structure was optimized for $n = 2$ to try and replicate the broad transition at 2840 cm^{-1}, but the geometry quickly converged to a structure where the $CH_3OH\cdots$18c6 hydrogen bond is not present (like **2-A** or **2-C**). In the free OH region, there is once again a singlet in the IRPD spectrum. The frequency position is ~3660 cm^{-1} which matches the higher-frequency component in $n = 2$. This would suggest a free OH stretch of a second-shell methanol, consistent with the structure of conformer **3-A**, which is the only conformer with a free OH stretch.

In the CH stretching region, the symmetric and asymmetric features continue to be relatively stable. The diminished distortion of the 18c6 macrocycle as a function of increasing solvation is also apparent in both DFT conformers for $n = 3$, which clearly show that the 18c6 configuration now resembles that of the gas-phase neutral configuration of 18c6. The evolution of the 18c6 ring from highly distorted (**0-A**) to the more neutral-like configuration for $n = 3$ is easily followed in the DFT structures shown in Figure 2. As the methanol network is extended in these systems, the distortion due to the $Mn^{2+}\cdots$18c6 interaction is weakened and the 18c6 ring opens up as the other noncovalent interactions began to complete. The experimental spectra also contain a feature at 2996 cm^{-1} which serves as a signature of this distortion. This feature decreases in relative intensity with increasing numbers of methanols (see Figures 3 and 5). This observation suggests that this band is due to a subset of methylene groups whose relationship to the Mn^{2+} changes with increasing methanol solvation numbers.

Conclusions

A custom ESSI source has allowed us to acquire high-quality experimental spectra of Mn^{2+}(18c6)$(CH_3OH)_{1-3}$ complexes, and it provides an avenue to study a wide variety of multiply charged metal ion systems. We have shown that 18c6 mitigates the unwanted effects of charge reduction/transfer and allows for stepwise solvation from the singly solvated state for the $M^{2+}-$18c6 complexes. Experiments in the CH stretching region and DFT calculations show that 18c6 stabilizes the charge of the dication by distorting the gas-phase neutral 18c6 geometry to maximize the favorable interactions of the macrocyclic oxygens with Mn^{2+}. With each stepwise addition of methanol this distortion is lessened, and by $n = 3$, 18c6 begins to assume a geometry close to its gas-phase neutral conformation. Experimental results in the OH stretching region reveal significant competition between the various noncovalent interactions present in these systems. These competing forces are first apparent in Mn^{2+}(18c6)$(CH_3OH)_2$ where the IRPD spectrum becomes complex in large part because both $CH_3OH\cdots$18c6 and $CH_3OH\cdots CH_3OH$ interactions are possible and compete with the $Mn^{2+}\cdots$18c6 interaction that was dominant in $n = 1$. The DFT harmonic vibrational frequency calculations hint that various different conformers are present in the experiment for $n = 2$. However, these calculations lack the ability to replicate a broad OH transition 2840 cm^{-1}, which may be due to anharmonic coupling between the in-plane bend overtone and a hydrogen-bonded OH transition. Future studies will aim at exploiting the stabilizing nature of the crown ether moiety to study other multivalent metal ions complexed with 18c6 and other polycylic ethers in solvated systems.

Acknowledgment. The authors wish to thank the National Science Foundation (Grants CHE-0415859 and CHE-0748874) for partial support of this research. Acknowledgment is made to the donors of the American Chemical Society Petroleum Research Fund for partial support of this research. Computational work was done on the NCSA Cobalt Supercomputer System (Award no. TG-CHE070097).

References and Notes

(1) Shvartsburg, A. A.; Siu, M. K. W. *J. Am. Chem. Soc.* **2001**, *123*, 10071.

(2) Spence, T. G.; Burns, T. D.; Guckenberger, G. B.; Posey, L. A. *J. Phys. Chem. A* **1997**, *101*, 1081.

(3) Spence, T. G.; Trotter, B. T.; Posey, L. A. *J. Phys. Chem. A* **1998**, *102*, 7779.

(4) Zhou, J.; Santambrogio, G.; Brummer, M.; Moore, D. T.; Woste, L.; Meijer, G.; Neumark, D. M.; Asmis, K. R. *J. Chem. Phys.* **2006**, *125*, 111102.

(5) Bush, M. F.; Saykally, Richard, J.; Williams, Evan R. *ChemPhysChem* **2007**, *8*, 2245.

(6) Bush, M. F.; Saykally, R. J.; Williams, E. R. *J. Am. Chem. Soc.* **2007**, *129*, 2220.

(7) Bush, M. F.; Saykally, R. J.; Williams, E. R. *J. Am. Chem. Soc.* **2008**, *130*, 9122.

(8) Bush, M. F.; Saykally, R. J.; Williams, E. R. *J. Am. Chem. Soc.* **2008**, *130*, 15482.

(9) Carnegie, P. D.; Bandyopadhyay, B.; Duncan, M. A. *J. Phys. Chem. A* **2008**, *112*, 6237.

(10) Walker, N. R.; Wright, R. R.; Stace, A. J. *J. Am. Chem. Soc.* **1999**, *121*, 4837.

(11) Yamashita, M.; Fenn, J. B. *J. Phys. Chem.* **1984**, *88*, 4451.

(12) Jayaweera, P.; Blades, A. T.; Ikonomou, M. G.; Kebarle, P. *J. Am. Chem. Soc.* **1990**, *112*, 2452.

(13) Takats, Z.; Wiseman, J. M.; Gologan, B.; Cooks, R. G. *Anal. Chem.* **2004**, *76*, 4050.

(14) Izatt, R. M.; Terry, R. E.; Haymore, B. L.; Hansen, L. D.; Dalley, N. K.; Avondet, A. G.; Christensen, J. J. *J. Am. Chem. Soc.* **1976**, *98*, 7620.

(15) Izatt, R. M.; Rytting, J. H.; Nelson, D. P.; Haymore, B. L.; Christensen, J. J. *Science* **1969**, *164*, 443.

(16) Armentrout, P. B. *Int. J. Mass spectrom.* **1999**, *193*, 227.

(17) Muzzalupo, R.; Nicoletta, F. P.; Trombino, S.; Cassano, R.; Iemma, F.; Picci, N. *Colloids Surf., B* **2007**, *58*, 197.

(18) Horwitz, E. P.; Dietz, M. L.; Fisher, D. E. *Solvent Extr. Ion Exch.* **1991**, *9*, 1.

(19) Shou, W. Z.; Browner, R. F. *Anal. Chem.* **1999**, *71*, 3365.

(20) Stace, A. J. *J. Phys. Chem. A* **2002**, *106*, 7993.

(21) Hirabayashi, A.; Sakairi, M.; Koizumi, H. *Anal. Chem.* **1994**, *66*, 4557.

(22) Nefliu, M.; Smith, J. N.; Venter, A.; Cooks, R. G. *J. Am. Soc. Mass Spectrom.* **2008**, *19*, 420.

(23) Lisy, J. M. *Int. Rev. Phys. Chem.* **1997**, *16*, 267.

(24) Deppmeier, B. J.; Driessen, A. J.; Hehre, T. S.; Hehre, W. J.; Johnson, J. A.; Klunzinger, P. E.; Leonard, J. M.; Pham, I. N.; Pietro, W. J.; Jianguo Yu; Kong, J.; White, C. A.; Krylov, A. I.; Sherrill, C. D.; Adamson, R. D.; Furlani, T. R.; Lee, M. S.; Lee, A. M.; Gwaltney, S. R.; Adams, T. R.; Ochsenfeld, C.; Gilbert, A. T. B.; Kedziora, G. S.; Rassolov, V. A.; Maurice, D. R.; Nair, N.; Shao, Y.; Besley, N. A.; Maslen, P. E.; Dombroski, J. P.; Dachsel, H.; Zhang, W. M.; Korambath, P. P.; Baker, J.; Byrd, E. F. C.; Voorhis, T. V.; Oumi, M.; Hirata, S.; Hsu, C. P.; Ishikawa, N.; Florian, J.; Warshel, A.; Johnson, B. G.; Gill, P. M. W.; Head-Gordon, M.; Pople, J. A. *SPARTAN 2002; SPARTAN 2002 SGI IRIX 64 (mips4) ed.* Irvine, CA, 2002.

(25) Frisch, M. J.; Trucks, G. W.; Schlegel, H. B.; Scuseria, G. E.; Robb, M. A.; Cheeseman, J. R.; Montgomery, J. A., Jr.; Vreven, T.; Kudin, K. N.; Burant, J. C.; Millam, J. M.; Iyengar, S. S.; Tomasi, J.; Barone, V.; Mennucci, B.; Cossi, M.; Scalmani, G.; Rega, N.; Petersson, G. A.; Nakatsuji, H.; Hada, M.; Ehara, M.; Toyota, K.; Fukuda, R.; Hasegawa, J.; Ishida, M.; Nakajima, T.; Honda, Y.; Kitao, O.; Nakai, H.; Klene, M.; Li, X.; Knox, J. E.; Hratchian, H. P.; Cross, J. B.; Adamo, C.; Jaramillo, J.; Gomperts, R.; Stratmann, R. E.; Yazyev, O.; Austin, A. J.; Cammi, R.; Pomelli, C.; Ochterski, J. W.; Ayala, P. Y.; Morokuma, K.; Voth, G. A.; Salvador, P.; Dannenberg, J. J.; Zakrzewski, V. G.; Dapprich, S.; Daniels, A. D.; Strain, M. C.; Farkas, O.; Malick, D. K.; Rabuck, A. D.; Raghavachari, K.; Foresman, J. B.; Ortiz, J. V.; Cui, Q.; Baboul, A. G.;

Clifford, S.; Cioslowski, J.; Stefanov, B. B.; Liu, G.; Liashenko, A.; Piskorz, P.; Komaromi, I.; Martin, R. L.; Fox, D. J.; Keith, T.; Al-Laham, M. A.; Peng, C. Y.; Nanayakkara, A.; Challacombe, M.; Gill, P. M. W.; Johnson, B.; Chen, W.; Wong, M. W.; Gonzalez, C.; Pople, J. A. *Gaussian 03*, B.04 ed.; Gaussian, Inc.: Pittsburgh, PA, 2003.

(26) Schaftenaar, G.; Noordik, J. H. *J. Comput.-Aided Mol. Des.* **2000**, 123.

(27) Gorelsky, S. I. *SWizard program*, http://www.sg-chem.net/ CCRI, University Of Ottawa, Ottawa, Canada, 2008.

(28) Irikura, K. K. *THERMO.PL*; National Institute of Standards and Technology: Gaithersburg, MD, 2002.

(29) Serrallach, A.; Meyer, R.; Gunthard, H. H. *J. Mol. Spectrosc.* **1974**, *52*, 94.

(30) Shimanouchi, T. *Tables of Molecular Vibrational Frequencies, Vol. I; NIST Chemistry WebBook, NIST Standard Reference Database Number 69,1972*; National Institute of Standards and Technology: Gaithersburg, MD, http://webbook.nist.gov, accessed June 2007.

(31) Noether, H. D. *J. Chem. Phys.* **1942**, *10*, 693.

(32) Robertson, W. H.; Weddle, G. H.; Kelley, J. A.; Johnson, M. A. *J. Phys. Chem. A* **2002**, *106*, 1205.

JP902381Y